Journal of
Water & Climate Change

IWA PUBLISHING

Journal of Water and Climate Change Vol 15 No 8, 4001 doi: 10.2166/wcc.2024.210

Characteristics of rainfall distribution induced by tropical cyclones using GSMaP data over the Vietnam region

Nga Pham Thi Thanh [a], The Doan Thi[a], Thuc Tran Duy[a], Kien Truong Ba[a], Hao Nguyen Thi Phuong[b], Hang Vu-Thanh[c], Ha Pham-Thanh[c], Nam Pham-Quang[c], Hang Nguyen Thu[d], Quan Tran-Anh[e] and Long Trinh-Tuan [f,*]

[a] Vietnam Institute of Meteorology, Hydrology, and Climate Change (IMHEN), Hanoi, Vietnam
[b] Vietnam National Space Center (VNSC), Vietnam Academy of Science and Technology (VAST), Hanoi, Vietnam
[c] Faculty of Hydrology, Meteorology and Oceanography, University of Science, Vietnam National University (VNU-HUS), Hanoi, Vietnam
[d] Vietnam National Center for Hydro-Meteorological Forecasting (VNHMF), Hanoi, Vietnam
[e] Department of Environmental, Hanoi University of Mining and Geology (HUMG), Hanoi, Vietnam
[f] Vietnam Academy for Water Resources (VAWR), Hanoi, Vietnam
*Corresponding author. E-mail: trinhtuanlong@hus.edu.vn; trinhtuanlong@gmail.com

NPTT, 0000-0003-4649-3544; LT, 0000-0003-0541-693X

ABSTRACT

Tropical cyclones (TCs) contribute significantly to rainfall along Vietnam's coast, yet their complex precipitation structures remain poorly resolved, hindering forecast skill. This study analyzes TC rainfall distributions over the Vietnam East Sea from 2000 to 2020. The Global Satellite Mapping of Precipitation (GSMaP) product provides precipitation estimates with 0.1° resolution at hourly intervals, enabling detailed structural characterization. Rainfall features are analyzed across TC intensities, motion vectors, landfall locations, and interactions with cold surge (CS) air masses. Results show that total coverage differences are less significant than the intensity variations in narrow inner core rainbands. Asymmetric rainfall distributions concentrate in the front-right quadrant but shift after landfall. Northern Vietnam observes higher TC frequencies, but southern regions experience heavier extreme rains. Additionally, CS intrusions substantially intensify eyewall convection and redirect TC precipitation. These structural sensitivities visible in GSMaP observations elucidate the dynamics modulating TC rainfall. Characterizing multi-scale interactions and precipitation processes aids in forecasting and impact assessment for these high-risk storms with complex regional behavior.

Key words: cold surge, GSMaP, tropical cyclone-induced rainfall, Vietnam East Sea

HIGHLIGHTS

- Total rainfall quantity and aerial coverage increase with greater tropical cyclone (TC) intensity.
- Interactions with land cause TC precipitation symmetries and intensities to evolve over time, and the total area of rainfall decreases post-landfall.
- Cold surges (CSs) appear to redirect and intensify rainfall within the inner core of TCs based on the analysis of TC–CS interactions.

GRAPHICAL ABSTRACT

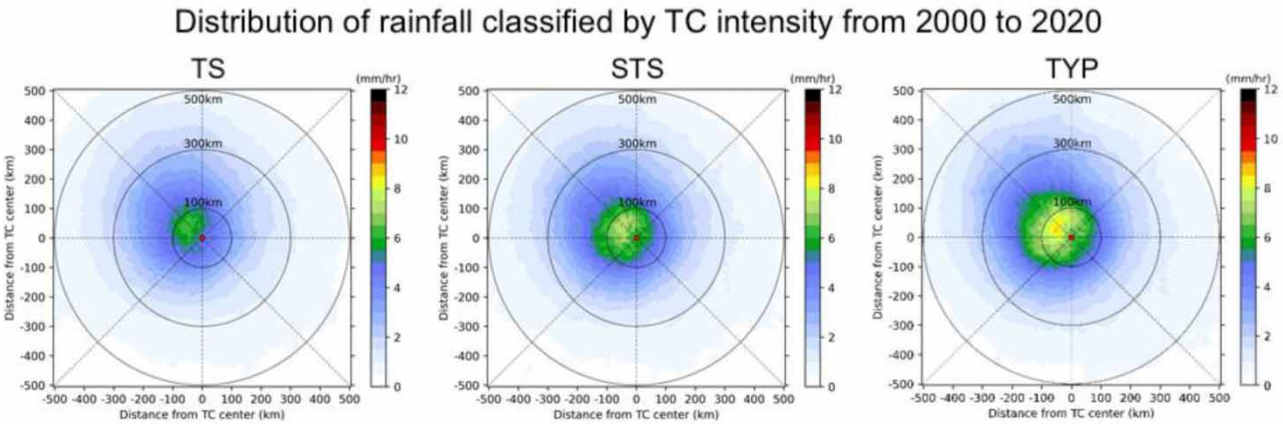

INTRODUCTION

Tropical cyclones (TCs) play a key role in shaping global rainfall patterns (Khouakhi *et al.* 2017; Ray *et al.* 2022). While they can replenish water resources and benefit agriculture, they can also cause devastating floods and landslides, causing widespread damage to people and infrastructure. To understand and predict their impact, researchers worldwide employ diverse tools, including sophisticated numerical models, rigorous data analysis, simulations, and direct on-the-ground observations (Walsh *et al.* 2016; Lavender & McBride 2021; Trinh *et al.* 2023).

Based on a 25-year data set from 1970 to 2014, consisting of best-track data and daily rainfall records from 18,607 global rain gauges, researchers found that the most significant TC-induced rainfall totals occurred in East Asia (>400 mm/year), northeastern Australia (>200 mm/year), the southeastern United States, and along the coast of the Gulf of Mexico (100–150 mm/year) (Khouakhi *et al.* 2017). TC rainfall accounted for 30–50% of the average annual rainfall in northwestern Australia, southeastern China, the northern Philippines, Baja California, and Mexico. Seasonal evaluation by Dare *et al.* (2012) revealed that about 40–50% of TC-induced rain occurs along the western coast of Australia in the islands of the south Indian Ocean in the austral summer, and in East Asia and Mexico in the boreal summer and fall. Regarding extremes, maximum rainfall was found in East Asia, Australia, and North and Central America (Khouakhi *et al.* 2017). Stream flow data and simulated runoff data from ERA5 reanalysis spanning 1979–2012 reveal significant contributions of TC-induced rainfall to annual floods. TCs account for over 40% of annual floods in coastal East Asia and Australia and over 25% in North America. TCs contribute more than 70% in Eurasia, over 60% in North America, and over 50% in South America and South Africa (Wang *et al.* 2021). Rainfall stations have demonstrated that TC-induced rainfall in Taiwan, and southeastern China averages around 500 mm/year, constituting 20–40% of the annual rainfall total (Ren *et al.* 2006). In Australia, during the peak of the TC season (from January to March), the TC rainfall contributes approximately 40% to the rainfall total in coastal regions west of 120°E, while, in December, it comprises approximately 60–70% of the total rainfall in areas west of 115°E (Dare *et al.* 2012). In the Philippines, ground and satellite observations indicate that TC rainfall accounts for 6% of the annual rainfall in the south and 54% in the north (Bagtasa 2017).

In recent decades, numerous studies worldwide have investigated the characteristics and complexity of TC. Early TC research highlighted the intricate structure of TC precipitation, which is often analyzed from radar images and exhibits variability from case to case (Miller 1958; Frank 1977; Marks 1985; Burpee & Black 1989). TC rainfall is typically organized by spiral bands that converge toward the TC center, referred to as rainbands, which can deform upon landfall (Wexler 1947). The spatial distribution of TC rainfall includes axisymmetric and asymmetric components (Chen & Li 2004), as evidenced by radar images in studies by Marks (1985) for Hurricane Allen (1980) and Burpee & Black (1989) for Hurricanes Alicia (1983) and Elena (1985). These studies observed variations in rainfall patterns, with the maximum rain rate shifting between different quadrants relative to the TC center, and terrain features like coastal lines and mountains significantly influence TC asymmetric rainfall, especially during landfall. The spatial distribution of TC rainfall is significantly influenced by wind velocity, vertical wind shear, moisture supply, and surface characteristics. Faster TC motion concentrates heavy rainfall in narrower bands near the track (Lonfat *et al.* 2004), while vertical wind shear tilts and asymmetrically enhances precipitation

downshear (Shapiro 1983). Furthermore, the moisture supply available to the TC significantly impacts the overall rainfall intensity. TCs over moisture-rich regions, such as warm ocean waters, can continue ingesting abundant moisture and fuel heavy precipitation (Zhang *et al.* 2013). Conversely, limited moisture supply can constrain rainfall amounts. Finally, surface characteristics, including land–ocean contrasts and topographic features, can modulate the spatial distribution of TC rainfall through processes like frictional convergence and orographic lifting (Lonfat *et al.* 2007; Yu *et al.* 2015). For instance, coastal regions and mountainous terrain often experience enhanced rainfall due to these effects.

In Vietnam, TC rainfall data from 138 stations (1979–2019) show varying impact, accounting for 10–20% of total annual rainfall in the northern and central regions, while remaining lower (less than 2%) in the southern region due to fewer TC occurrences (Pham-Thanh *et al.* 2020). The highest TC rainfall is recorded in the central region in July. Recent observation records (2018–2022) highlight significant TC rainfall contributions during major heavy rain events, ranging from 15 to 37%. TCs frequently interact with East Asian cold surges (CSs) over Vietnam, which dramatically enhances rainfall and causes extreme flooding events (Wang *et al.* 2015; Trinh *et al.* 2020; Gori *et al.* 2022). The complex interplay between TCs and CSs results in a significant modulation of moisture transport and convergence, leading to heavy precipitation over coastal Vietnam. Recent studies indicate that extreme rainfall events in Central Vietnam involve TC–CS interactions (Yokoi & Matsumoto 2008; Do *et al.* 2020; Wolf *et al.* 2020). As climate variability increases, improved forecasting of these compound events is crucial for disaster risk reduction in this vulnerable region.

Satellite-based precipitation estimates have proven invaluable for understanding TC structure and evolution, especially in data-sparse oceanic regions. The Tropical Rainfall Measuring Mission (TRMM) satellite's precipitation radar has been leveraged to reveal fine-scale structural details related to TC eyes, eyewalls (known as the ring of intense thunderstorms surrounding the eye of a TC), and rainbands. This reveals how vertical profiles vary by storm quadrant and environmental wind shear (Hence & Houze 2011). Chen *et al.* (2006) found that vertical wind shear over 5 m/s significantly impacted TC precipitation asymmetry, while TC motion was important in low-shear environments. Similarly, Gao *et al.* (2017) found that incorporating total precipitable water content, in addition to TC intensity, substantially improved model landfall precipitation forecasts. Analysis of global TC core precipitation generally shows agreement with a Gaussian distribution pattern, where precipitation intensity is highest at the center and decreases radially outward (Huang & Chen 2019). However, significant variability exists across different ocean basins due to factors such as environmental conditions, geographic features, and landmass configurations surrounding each basin. Despite the Gaussian model serving as a reference, the observed deviations highlight the complexity and diversity of TC precipitation structures globally. Other studies have utilized the high-resolution precipitation estimates from the Global Satellite Mapping of Precipitation (GSMaP) product (Kubota *et al.* 2020). Richardson *et al.* (2022) analyzed GSMaP data for North Pacific TCs, finding a good agreement with ground observations and revealing asymmetric outer rainband structures modulated by vertical wind shear. Examining typhoons in 2004, Lonfat *et al.* (2004) showed that rain area and volumetric rain content scaled with storm intensity, providing new metrics for monitoring TC strength. For landfalling TCs, blended GSMaP with gauge data improve quantitative precipitation forecasting (Richardson *et al.* 2022). Huang & Chen (2019) used GSMaP to study precipitation structures of recurring TCs in the Western North Pacific, detecting increased rainfall in the outer rainbands as storms recurved poleward. Beyond TCs, Aonashi *et al.* (2009) described the full GSMaP processing system that merges passive microwave and infrared satellite observations to produce high-resolution global precipitation maps. Evaluation studies by Miyato *et al.* (2021) demonstrated GSMaP's overall skill in capturing precipitation distribution and timing compared to ground radar and rain gauge networks across Japan. The fusion of TRMM's detailed structural observations and GSMaP's high-resolution rainfall estimates highlights the value of satellite platforms for both advancing TC's physical understanding and improving operational forecasts.

TCs and floods account for over 90% of natural disaster damages in Vietnam (MONRE 2021; Takagi *et al.* 2023). As climate conditions in Vietnam are projected to worsen by the end of the 21st century (Trinh-Tuan *et al.* 2019a; Tran *et al.* 2022; Tran-Anh *et al.* 2022, 2023), studying changes in TC rainfall distributions over Vietnam will become increasingly critical. Accurately forecasting TC rainfall remains challenging, especially as TCs approach landfall, due to complex interactions with terrain and weather systems that alter rainfall patterns (Cheung *et al.* 2018; Ray *et al.* 2022). Utilizing satellite data can help reconcile these discrepancies and improve process understanding. Satellite rainfall data provide extensive spatial coverage and improved accuracy to enhance understanding of TC rainfall structures over Vietnam (Trinh-Tuan *et al.* 2019b; Pham & Vu 2020).

This study leverages high-resolution precipitation estimates from the GSMaP data set to conduct a comprehensive investigation of TC rainfall distributions over the Vietnam East Sea (VES) region. A key focus is characterizing the spatial

patterns and asymmetries in TC rainfall fields by categorizing them based on influential factors such as TC intensity, storm motion direction, landing location along the Vietnamese coastline, interactions with CS systems, and the evolution of rainfall distribution before and after landfall. The primary objectives are to systematically characterize the variability in TC rainfall features and their asymmetric structure across these influential factors, deepen our understanding of the mesoscale precipitation processes governing the evolution and distribution of rainfall in landfalling TCs over the complex coastal environment of Vietnam, and utilize the observational insights to enhance operational forecasting capabilities for more accurate predictions of TC rainfall distributions and associated hazards that can severely impact Vietnam. The insights gained from this multi-faceted analysis will provide valuable information to support TC and flood forecasting efforts in the VES, as well as to assess the potential rainfall impacts and hazards associated with landfalling systems affecting Vietnam.

DATA AND METHOD

TC data

The best-track data of TCs are used from the Regional Specialized Meteorological (RSMC) of Tokyo – Typhoon Center during the period 2000–2020 (Kunitsugu 2012). The historical TC records provide information on the position of the TC center (LAT, LONG), maximum sustained winds (V_{max}), minimum central pressure (P_{min}), the radius of maximum winds, TC track name, and 6-hourly temporal resolutions (0000UTC, 0600UTC, 1200UTC, and 1800UTC). This study focuses on TCs that originated in the central Pacific Ocean and tracked westward toward the VES region during the period 2000–2020. Specifically, we consider TCs that passed through the domain bounded by 5–25°N latitude and 145–120°E longitude. This domain encompasses the entire westward journey of the TCs from their formation in the central Pacific until they reached the VES and coastal areas of Vietnam. Within this domain, a total of 177 TCs were identified and tracked during the 2000–2020 period. These 177 TCs provided 5,044 instantaneous precipitation observations associated with their passage through the domain.

TC intensity is typically classified internationally using the Saffir–Simpson hurricane wind scale, with storms categorized into five levels (CAT 1–5) based on their maximum sustained wind speeds. However, in Vietnam, TC intensity is traditionally divided into levels 8–12 and greater than 12 on the Beaufort wind scale. To ensure consistency with previous studies (Camargo & Sobel 2005; Wang & Zhou 2008) and facilitate comparison with international data, we categorized TC intensity into three classes based on maximum sustained wind speeds: Tropical Storm (TS) (34–48 knots), Severe Tropical Storm (STS) (48–63 knots), and Typhoon (TYP) (over 63 knots), aligning with the international Saffir–Simpson scale.

To classify TC-landing regions along the Vietnamese coastline, we followed Vietnam's standard division outlined by the Ministry of Natural Resources and Environment, which divides the VES into 10 zones (MONRE 2016). Zones 1–6 cover the coastal region of Vietnam. However, due to the smaller size and fewer historical TC landfalls in zones 5 and 6 compared to zones 1–4, we combined these zones into zone 4 to form a single region (referred to as R4) to more accurately reflect regional TC impacts. The four regions considered in this study are defined as follows (Figure 1): R1 from Quang Ninh to Nam Dinh (21.6–19.9°N); R2 from Thanh Hoa to Quang Binh (20–16.9°N); R3 from Quang Tri to Quang Ngai (17–14.6°N); and R4 from Binh Dinh to Ca Mau (14.7–8.6°N).

Satellite rainfall data

The GSMaP is a global rain rate data set that provides hourly measurements with a resolution of $0.1° \times 0.1°$, encompassing the expansive region between 60°N and 60°S. It is created through the collaboration of multiple satellites, including Global Precipitation Measurement satellites and passive microwave and infrared radiometers on geostationary satellites, developed by Japanese scientists under the sponsorship of the Japan Science and Technology Agency (JST) and the Japan Aerospace Exploration Agency (JAXA) (Kubota *et al.* 2007; Aonashi *et al.* 2009; Ushio *et al.* 2009). In this study, we utilized the standard Version 6 of GSMaP data, known as GSMaP_MKV, spanning the period 2000–2020. The GSMaP_MKV data set is a bias-corrected product that employs a Kalman filter model to refine precipitation rate estimates (Ushio *et al.* 2009). This enhancement is achieved by leveraging atmospheric moving vectors derived from successive infrared images. While this global data set offers rainfall data for any location worldwide, the GSMaP_MKV data are limited to the period from March 2000 to the present. It provides a maximum spatial resolution of $0.1° \times 0.1°$ (approximately 10 km × 10 km) in its highest resolution product. The effectiveness of GSMaP in capturing rainfall patterns has been validated in Vietnam and its coastal areas (Nodzu *et al.* 2019; Trinh-Tuan *et al.* 2019b). GSMaP enables detailed tracking and analysis of rainfall patterns, trends, and climate variations due to its fine resolution and coverage. The GSMaP data can be freely downloaded from the website of JAXA: http://sharaku.eorc.jaxa.jp/GSMaP/.

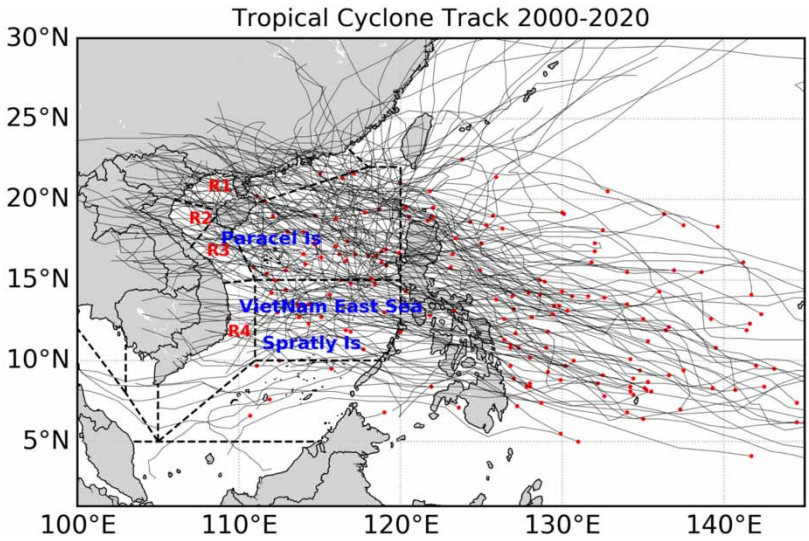

Figure 1 | Defined landing regions (dashed polygons) and best-track data during 2000–2020. Red dots signify the initiation points of TC tracks, while solid lines trace their movement paths. The landing regions of TCs in Vietnamese territory are highlighted in red and are labeled as R1–R4, ascending in number from north to south.

ERA5 represents the fifth major global atmospheric reanalysis developed by the European Center for Medium-Range Weather Forecasts (ECMWF) (Hersbach *et al.* 2020). With 0.25° spatial resolution and hourly outputs, ERA5 incorporates observations, models, and data assimilation to generate consistent estimates of historical weather variables like rainfall. Here, ERA5 wind data were utilized over Vietnam from 2001 to 2020 to complement the GSMaP rainfall analysis in cases of CS–TC interaction.

In this study, we categorized TC rainfall into three intensity types using specific thresholds: light rain (>0.5 mm/h), moderate rain (1–5 mm/h), and heavy rain (>5 mm/h). The light rain threshold was chosen to capture even minimal precipitation, ensuring comprehensive coverage detectable by sensors. Moderate rain represents the predominant intensity range observed during TC events in our study area, encompassing moderate rainfall rates commonly associated with TC activity. Meanwhile, the heavy rain threshold, exceeding the 95th percentile level in the VES during TC passages, highlights the most extreme precipitation events, indicating the potential for hazardous rainfall conditions. Comparing the high-resolution patterns seen in GSMaP observations and robust climatological trends from the ERA5 reanalysis facilitates deeper insights into TC precipitation variability.

Reorient the direction of TC motion

To facilitate the spatial analysis of rainfall distributions, all TC tracks in Figure 1 are adjusted at each timestep to reorient the direction of TC motion toward the west. Specifically, the TC center locations are rotated to align the heading vector with 270° (directly westward, Figure 2). This processing keeps the rainfall patterns locked in a consistent frame of reference as the TC naturally changes direction during their tracks (Lonfat *et al.* 2004). This standardized rotation aligns precipitation structures with the translated TC center for the characterization of TC-relative distributions. By removing variability in the motion azimuth, comparisons of rainfall morphology patterns among different TCs and timesteps are simplified. The TC-relative structure is maintained while enabling easier characterization of spatial features through consistent left, right, front, and rear quadrants across all time points. This process refines the examination of rainfall morphology concerning TC center, motion, and related factors.

Determining the association between TCs and CSs

The CS refers to a periodic southward advancement of cold, midlatitude air along the eastern flank of the Tibetan Plateau in the lower troposphere, primarily occurring during the November–March period. Numerous studies have shed light on the spatio-temporal patterns of CSs. The CS northerly wind signal first appears near 40°N in northern China associated with a trough–ridge system aloft (Wu & Chan 1997; Chen *et al.* 2015; Perşoiu *et al.* 2019), following the strengthening of the

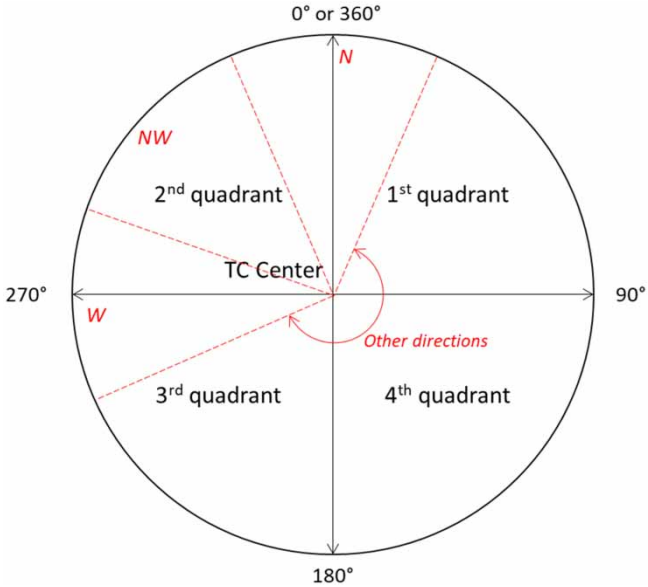

Figure 2 | Rainfall quadrant distribution and TC movement direction.

Siberian High (Zhang *et al.* 1997). Subsequently, the CS signal progresses southward into the tropics within a few days (Wu & Chan 1995; Compo *et al.* 1999). The CS's arrival is characterized by a pronounced increase in surface pressure, robust northerly winds, and a decrease in temperature (Perşoiu *et al.* 2019). After reaching the VES, the CS enhances convective activity over the VES, Borneo Island, and at times, the Maritime Continent in the Southern Hemisphere (Chang *et al.* 2005). Consequently, the CS also impacts the dynamic structure of TCs as well as the distribution of rainfall induced by TCs (Cheung *et al.* 2018).

To investigate the influence of CS on TC rainfall distributions, this study adopts specific criteria to identify TCs interacting with CS events, as defined by Chang *et al.* (2005) and Yokoi & Matsumoto (2008). The center of the TC must fall within a 500 km radius of the longitudinal line representing the cold air mass boundary. Two thresholds are used: (1) CS15 based on the 15°N line (3-day mean) and (2) CS20 on the 20°N line (1-day mean). Specifically, CS15 requires a 925-hPa meridional wind anomaly of less than −3.1 m/s averaged from 110°E to 120°E at 20°N. CS20 requires 925-hPa meridional winds to be less than −8 m/s averaged from 110°E to 117.5°E at 15°N. The CS15 threshold delineates a more robust CS, while CS20 captures all cold air masses. TCs that do not meet either criterion are considered neutral cases, not influenced by CSs. This integrated framework facilitates the examination of rainfall distribution when TC interacts with cold air masses.

RESULTS AND DISCUSSION

Rainfall distribution classified by TC intensity

Figure 3(a) illustrates both the cumulative duration and the associated rainfall patterns across different TC intensities observed in the Pacific Ocean from 2000 to 2020. Throughout this timeframe, storms of TC intensity or higher were documented for a total of 5,044 timesteps. Among these, TS accounted for 46.3% of the total duration, followed by STS at 31.6% and TYP at 22.1%. Total rainfall quantity and aerial coverage increase with greater storm intensity, reflecting larger moisture convergence zones, albeit with only minor differences in rainfall footprint areas (>0.5 mm/h) between classes (Table 1), covering 78.2% (TS) to 80.9% (TYP) of the 500 km radius storm area. However, peak rainfall becomes more intensely focused on the storm center at higher intensities, concentrated in the eyewall region. There are significant differences in extreme rainfall intensities (>5 mm/h) between TC types within 500 km of the TC center, with a coverage of 6.1% for TYP, 4% for STS, and 1.8% for TS. Significant rainfall asymmetry biased toward the front-right (second) quadrant occurs for all TC intensity groups, aligning with extensively documented patterns (Rodgers *et al.* 1994; Lonfat *et al.* 2004; Chen *et al.* 2006; Kepert 2006). This reflects the combination of opposing cyclonic flow and storm motion vectors that enhance uplift and moisture

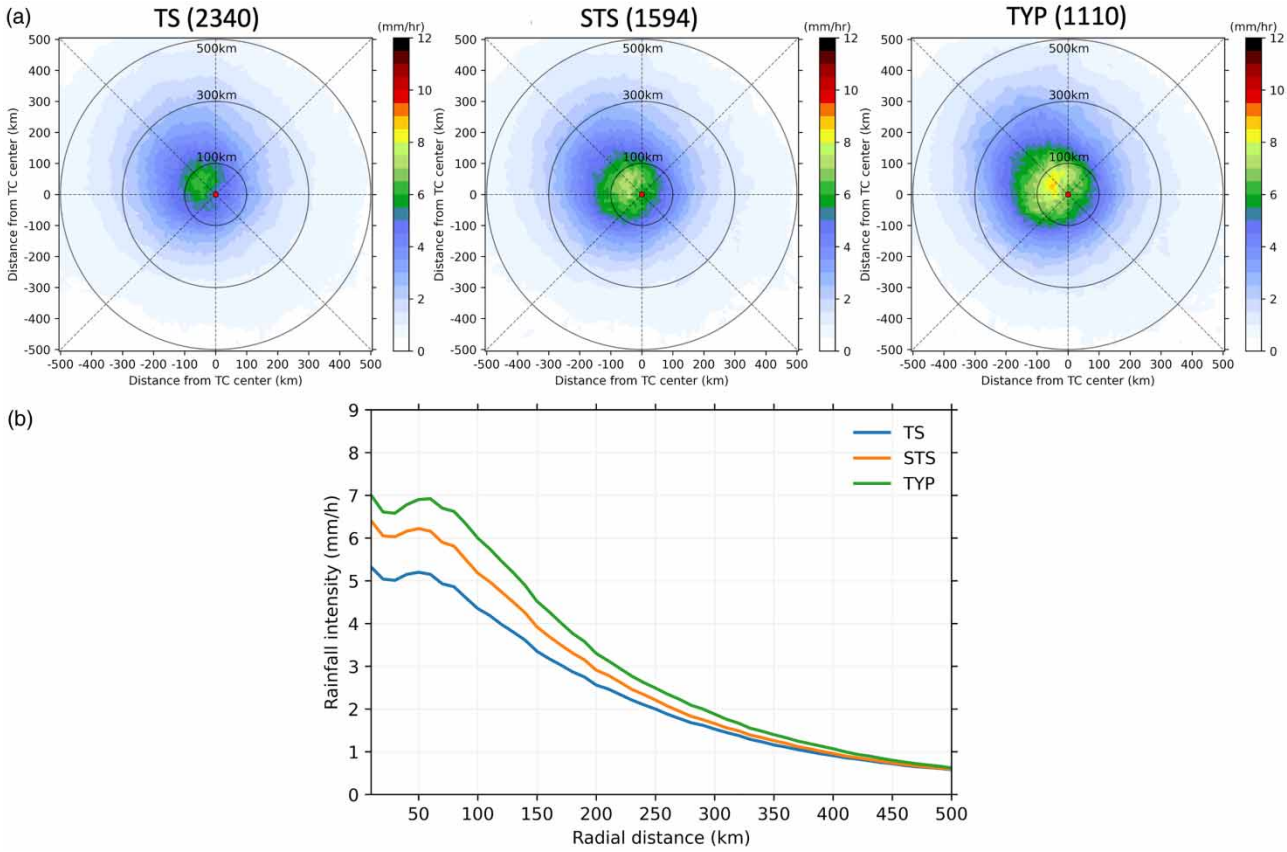

Figure 3 | (a) Distribution of rainfall classified by TC intensity from 2000 to 2020. The numbers given in brackets indicate the total number of timesteps for each TC intensity category formed in the Western Pacific Ocean. (b) Rainfall intensity distribution is relative to the distance from the TC center, categorized by TC intensity.

Table 1 | Percentage of the area covered by rainfall under different TC intensities within a 500 km radius of the storm eye

Rainfall intensity	TS	STS	TYP
Light	78.2	78.4	80.9
Moderate	41.8	44.5	48.2
Heavy	1.8	4.0	6.1

convergence downshear-right. Frictional convergence may provide additional enhancement (Shapiro 1983). The first, third, and fourth quadrants exhibit successively lower mean rainfall rates.

Analysis of the full radial distribution of rainfall (Figure 3(b)) reveals peak intensities within 10 km of the eyewall for all TCs, representing the zone of strongest convection and inflow (Houze 2010). Moving radially outward from the eyewall, rainfall intensity gradually diminishes between 10 and 50 km before exhibiting secondary maxima around 60–70 km from the storm center. These secondary maxima highlight the presence of outer rainband convection, a significant structural feature of TC precipitation distributions. Outer rainbands are organized, spiraling bands of deep convection that extend outward from the TC's inner core region, typically observed between 100 and 300 km from the center. While the eyewall remains the primary precipitation feature, outer rainbands can substantially contribute to the TC's total rainfall output and often produce intense precipitation rates. The formation and maintenance of outer rainband structures result from several dynamical mechanisms, including the upscale growth of convective elements through vortex stretching and vorticity organization (Qin

et al. 2021), interactions between the TC's vortex and environmental factors like vertical wind shear and upper-level troughs inducing asymmetries (Ying & Zhang 2012), and frictional convergence near the TC's outer circulation, enhancing convection (Martinez *et al.* 2020). Distinctions between TS, STS, and TYP are most apparent within 300 km, reflecting varying precipitation patterns across TC intensities. As the TC intensity increases, so do the rain rates in the critical eyewall and rainband regions, highlighting the connection between precipitation processes and storm dynamics (Hence & Houze 2011). However, the peak outer band location seems insensitive to intensity, contrasting some studies (Didlake & Houze 2013).

Rainfall distribution classified by the landing region

Figure 4(a) provides an overview of the total TC occurrences alongside rainfall distributions across different regions of Vietnam. Despite smaller areas, the northern regions R1 and R2 experience significantly more TC events (1,638 timesteps) than southern R3 and R4, which total 926 timesteps. This reflects higher climatological TC susceptibility in northern areas. While average rainfall area percentages are lower in R1/R2 (35.8%, 17.1%) versus R3/R4 (21.8%, 25.3%), the fraction of intense rain rates exceeding 5 mm/h in R1 (3.9%) and R2 (4.1%) slightly exceeds R3 (3.3%) and R4 (3.7%) (Table 2). This indicates that the complex coastal geography of the Gulf of Tonkin amplifies rainfall, as no terrain barriers exist in southern regions to disrupt TCs. Additionally, as latitude decreases from north to south, rainfall asymmetry shifts from concentrated in the second quadrant to a broader first/second quadrant distribution. This aligns with modeling studies, which shows that latitude significantly modulates TC precipitation distributions via Coriolis and environmental wind shear impacts (Lonfat *et al.* 2004; Chen *et al.* 2006). It further highlights the sensitivity of regional rainfall patterns to geographic effects.

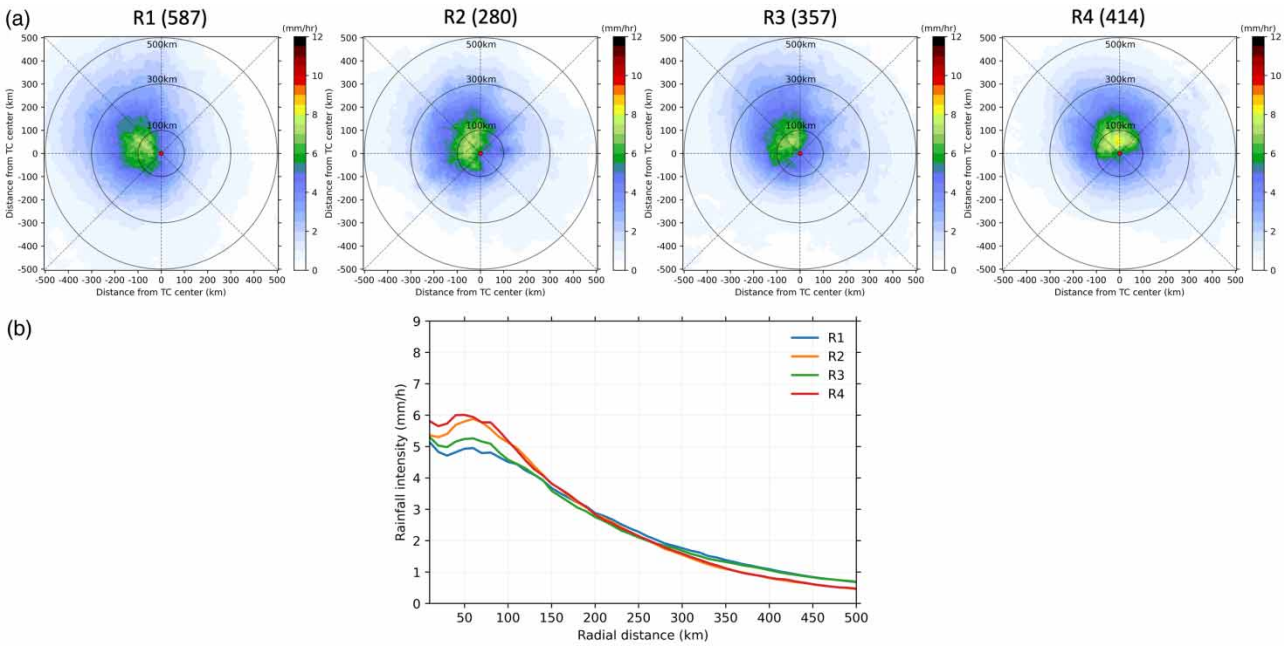

Figure 4 | Same as Figure 3, but the rainfall distribution is categorized based on the landing region.

Table 2 | Same as Table 1, but the rainfall distribution is categorized based on the landing region

Rainfall intensity	R1	R2	R3	R4
Light	78.3	67.6	85.2	66.6
Moderate	46.8	37.5	44.5	39.8
Heavy	3.9	4.1	3.3	3.7

Despite slightly lower fractions of intense rain rates compared to R1/R2, Figure 4(b) makes it clear that the extent of extreme rainfall occurring during TC events is greater in the southern R4 region versus northern areas (R1–R3). This disparity is likely due to higher atmospheric moisture content from proximity to warm ocean waters, weaker vertical wind shear favoring better-organized convection, and flatter coastal terrain in southern regions compared to the north. Southern Vietnam's location allows for longer TC overland trajectories, sustained moisture uptake, and potential enhancement from interactions with moisture-laden monsoonal flows, all contributing to higher rainfall accumulations during TC passages toward lower latitudes. Overall, northern Vietnam faces higher cyclone occurrence frequency, but southern regions experience greater extreme precipitation magnitudes.

Rainfall distribution classified by the TC-moving direction

Analysis of TC movement directions and precipitation patterns over 2000–2020 is shown in Figure 5(a). The three dominant directions were due west (56.7% of occurrences), northwest (21.1%), and north (5.4%), while other headings comprised 16.8% (Figure 5(a)). Total rainfall coverage ranging from 72.9 to 79% was quite similar across motion vectors (Table 3), indicating that translation exerts secondary control on precipitation area. However, directional asymmetry emerged in heavy rainfall distributions. West- and northwest-moving TCs produced the most intense rain rates (3.4 and 3.2% coverage, respectively), focused in the downshear-right second quadrant. This aligns with vertical wind shear and storm motion vector combinations enhancing convection in these regions (Chen *et al.* 2006; Wingo & Cecil 2010). Northward-moving TCs featured more symmetric precipitation. Given the prevalence of west-to-northwest storm headings in the Western Pacific, climatological rainfall peaks in this region. Although there are variations in asymmetry among storm motion vectors, the overall distribution of intensity radiates similarly across the predominant directions (Figure 5(b)).

Rainfall distribution before and after landing

Analysis of TC precipitation features before and after landfall reveals significant evolution (Figure 6(a)). More rainfall occurs pre-landfall, concentrated in the front-right quadrant, resembling distributions over the ocean due to vertical wind shear and motion vector interactions (Chen *et al.* 2006). Post-landfall, moderate rain rates become scattered across quadrants until dissipating as the storm decays inland. The areal coverage of total precipitation gradually decreases from 72% at L – 24 h to 53.6% at L + 12 h (Supplementary Table A1), while heavy rainfall peaks at 6.1% 12 h before landfall, then it rapidly drops

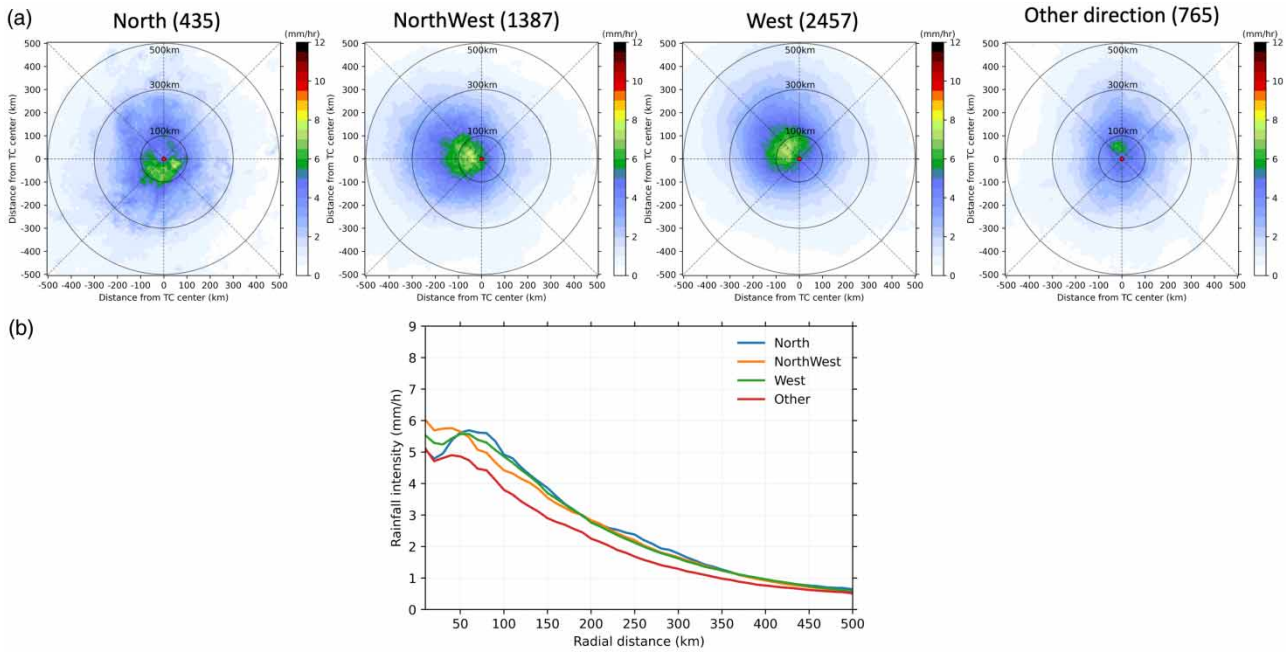

Figure 5 | Same as Figure 3, but the rainfall distribution is categorized based on the TC-moving direction.

Table 3 | Same as Table 1, but the rainfall distribution is categorized based on the TC-moving direction

Rainfall intensity	North	Northwest	West	Other
Light	79.2	74.8	74.7	72.9
Moderate	48.5	41.7	43.2	35.7
Heavy	2.5	3.2	3.4	0.6

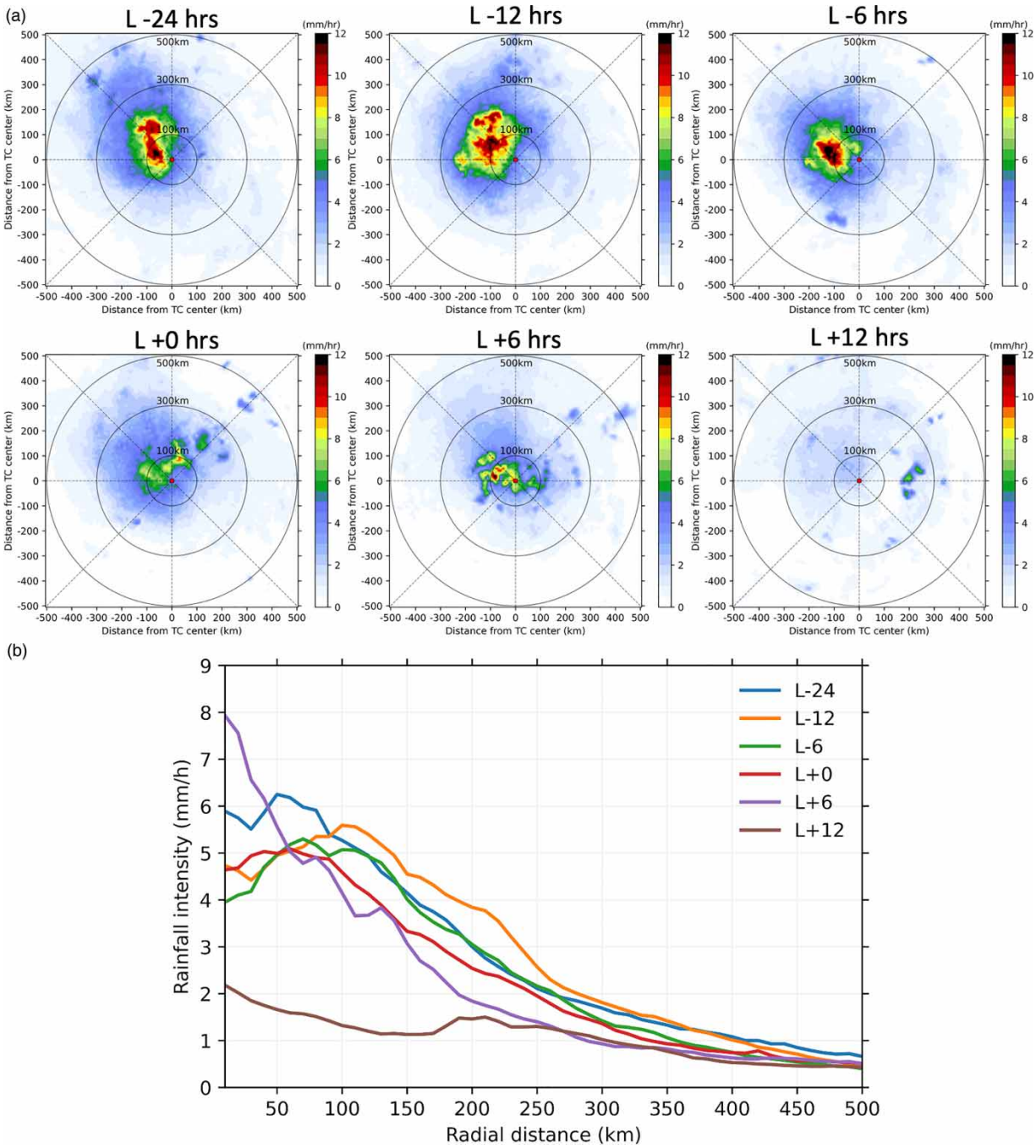

Figure 6 | Same as Figure 3, but the rainfall distribution is categorized based on the landing time of TCs.

afterward. This aligns with inner core intensity weakening over land (Kuo *et al.* 1991). However, even 24 h post-landfall, rainfall exceeding 1 mm/h still covers 24.6% of the area. This highlights orographic lifting from Vietnam's mountainous terrain sustaining convection despite dissipating dynamics (Lin *et al.* 2001). Ultimately, interactions with land cause precipitation symmetries and intensities to evolve. While the total rainfall in the area decreases post-landfall, terrain effects and residual moisture maintain a significant coverage of lighter precipitation. Figure 6(b) analysis reveals maximum rainfall rates occur approximately 12 h before landfall time at a distance of 90–120 km from the TC radius.

Rainfall distribution under the influence of CSs

TC rainfall patterns demonstrate a notable sensitivity to interactions with CSs – the intrusion of cold, dry air masses at low levels (Figure 7(a)). Compared to neutral TCs, cases meeting CS criteria CS15 (strong surges) and CS20 (all surges) exhibited important changes. As illustrated in Supplementary Table A2, total precipitation coverage was greatest for neutral storms (85.2%) versus CS15 (76.1%) and CS20 (81.0%). However, this largely reflected expansive areas of lighter rain rates. Intense inner core rain rates (heavy rain within a 500 km radius) increased substantially for both CS15 (3.4%) and CS20 (2.5%) relative to neutral TCs (1.6%). As cold and dry air interacts with the TC vortex edge, it may absorb moisture surrounding the TC while dynamically forcing stronger updrafts in the eyewall region, leading to an enhanced rainfall rate in the TC center.

In CS15 cases, rainfall concentrates in the first/second quadrants, while CS20 and neutral TCs peak in the second quadrant. CS15 shows the most intense pattern, particularly within the inner core. The enhanced convection likely arises from the upward motion and stretching of the storm system due to the positive rotation of winds brought about by the CS (Heo *et al.* 2018; Tan *et al.* 2023). Tighter meridional gradients in CS15 versus CS20 (Chang *et al.* 2005; Yokoi & Matsumoto 2008) support stronger interactions. The CS appears to redirect and intensify rainfall within the inner core of TCs, as depicted in Figure 7(b).

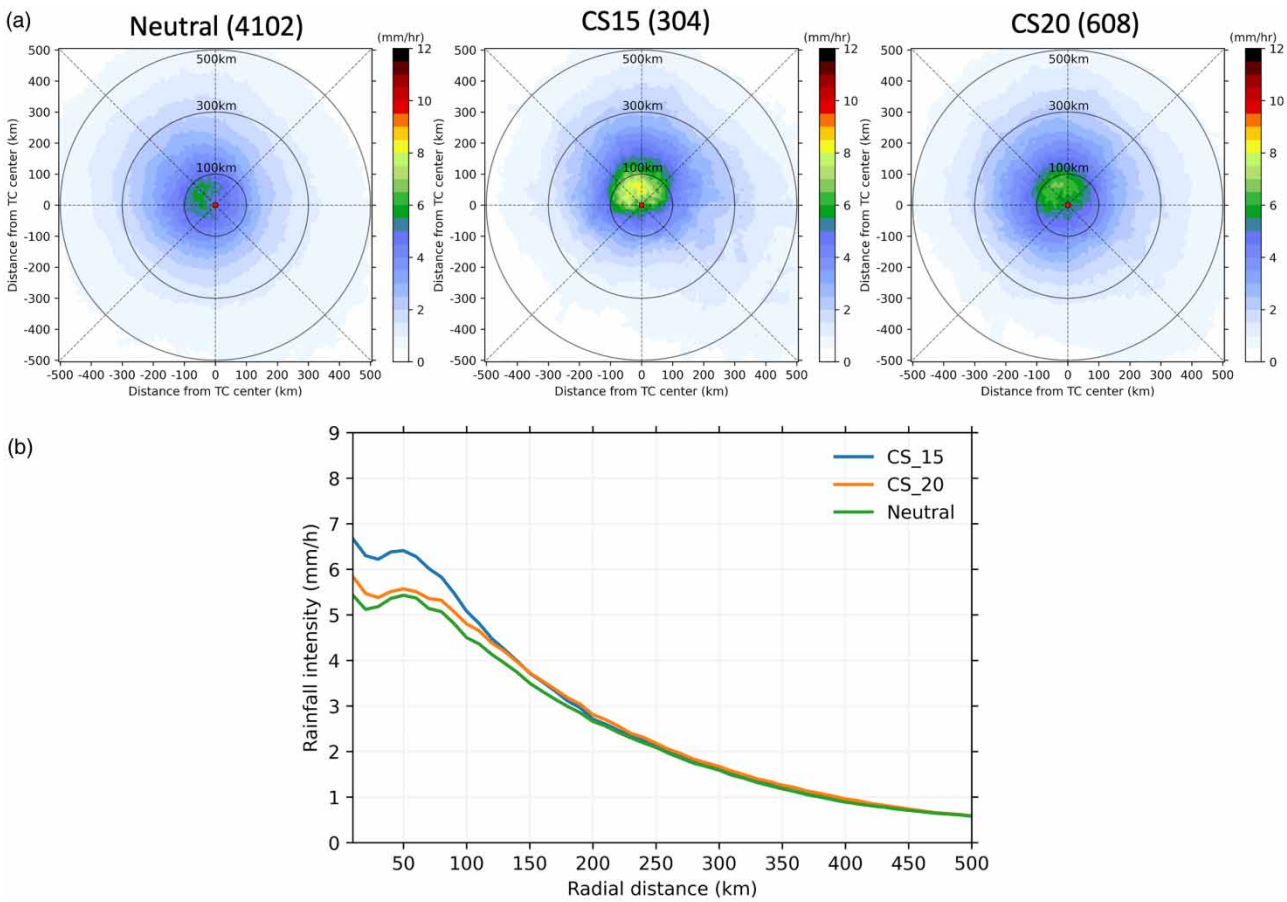

Figure 7 | Same as Figure 3, but the TC rainfall distribution is categorized based on the influence of CSs.

Overall, it is evident that TC rainfall is significantly influenced by interactions with environmental air masses like CSs. The structural changes visible in high-resolution GSMaP data provide new observational evidence elucidating the underlying dynamics modulating TC morphology.

CONCLUSIONS

This study analyzed TC rainfall distributions over the Vietnam region from 2000 to 2020 using GSMaP precipitation and ERA5 reanalysis data. Rainfall features were characterized across categorizing by TC intensities, motion vectors, landfall regions, and interactions with CS systems.

Key findings highlight the scaling of total rainfall coverage with TC intensity, while peak rain rates increasingly concentrate around the eyewall region at higher intensities. Rainfall distribution shows asymmetry, with higher precipitation observed in the front-right quadrant due to the combined effects of cyclonic flow and storm motion vectors, enhancing uplift and moisture convergence. However, distinct regional variations are observed, which are tied to geographical influences and climatological factors. Northern Vietnam experiences more frequent TC occurrences, but southern regions exhibit heavier extreme rainfall events. This disparity is attributed to higher atmospheric moisture content, weaker vertical wind shear favoring better-organized convection, and flatter coastal terrain in southern areas compared to the mountainous north. Furthermore, southern Vietnam's location allows for longer overland TC trajectories, sustained moisture uptake, and potential enhancement from interactions with moisture-laden monsoonal flows, collectively contributing to higher rainfall accumulations during TC passages toward lower latitudes.

Rainfall distributions undergo evolution significantly before and after landfall. Pre-landfall, rainfall concentrates in the front-right quadrant, resembling patterns over the ocean due to vertical wind shear and motion vector interactions. Post-landfall, moderate rain rates become scattered across quadrants until dissipating as the storm decays inland. However, even 24 h after landfall, rainfall exceeding 1 mm/h still covers a substantial area, highlighting the role of Vietnam's mountainous terrain in sustaining convection through orographic lifting despite dissipating dynamics. Notably, interactions with CS air masses substantially intensify convection within the TC inner core. GSMaP observations reveal that strong CS cases (CS15) exhibit enhanced rainfall rates and a concentration of precipitation in the first/second quadrants, while weaker CS cases (CS20) and neutral TCs peak in the second quadrant. The structural changes visible at fine scales in GSMaP data provide new observational evidence elucidating the dynamics modulating TC morphology due to synoptic-scale interactions.

This integrated analysis combining high-resolution satellite rainfall estimates and reanalysis climatology provides an improved understanding of mesoscale precipitation processes in TCs making landfall in complex coastal environments like Vietnam. Characterizing structural sensitivities and regional variations aids in forecasting these high-impact events. The findings offer insights into mesoscale processes governing TC precipitation, such as outer rainband formation and evolution, which can be incorporated into operational forecast models to enhance rainfall predictions. Additionally, the analysis can inform tailored forecast products, risk assessments, and hazard mapping specific to the region, ultimately improving disaster preparedness and resilience against TC-related rainfall hazards. While the methodology offers a framework applicable to other TC regions worldwide, acknowledging potential limitations is crucial. Factors such as environmental conditions, geographical influences, data availability, climatological differences, and temporal changes may require adjustments. Region-specific validations and local expertise incorporation are recommended for appropriate application in new TC regions.

ACKNOWLEDGEMENTS

The authors acknowledge JAXA for providing GSMaP data. TC data were sourced from RSMC Tokyo – Typhoon Center, and ERA5 data were provided by the ECMWF. The authors thank the editor and three reviewers for their valuable comments and suggestions, which significantly enhanced the quality of this manuscript.

AUTHORS' CONTRIBUTIONS

N.P.T.T. and L.T.-T. conceptualized the research. L.T.-T., Q.T.-A., T.D.T., and N.P.-Q. processed the data and conducted the analysis. All authors discussed the results and contributed to the writing of the manuscript.

FUNDING

This study was conducted with full support from Vietnam's National Project 562 (Grant Number ĐTĐL.CN-59/21), which is funded by the Vietnam Ministry of Science and Technology.

DATA AVAILABILITY STATEMENT

All relevant data are included in the paper or its Supplementary Information.

CONFLICT OF INTEREST

The authors declare there is no conflict.

REFERENCES

Aonashi, K., Awaka, J., Hiroshe, M., Kozu, T., Kubota, T., Liu, G., Shige, S., Kida, S., Seto, S., Tahahashi, N. & Takayabu, Y. N. 2009 GSMaP passive microwave precipitation retrieval algorithm: Algorithm description and validation. *Journal of the Meteorological Society of Japan* **87**, 119–136. https://doi.org/10.2151/jmsj.87A.119.

Bagtasa, G. 2017 Contribution of tropical cyclones to rainfall in the Philippines. *Journal of Climate* **30**, 3621–3633. https://doi.org/10.1175/JCLI-D-16-0150.1.

Burpee, R. W. & Black, M. L. 1989 Temporal and spatial variations of rainfall near the centers of two tropical cyclones. *Monthly Weather Review* **117** (10), 2204–2218. https://doi.org/10.1175/1520-0493(1989)117.

Camargo, S. J. & Sobel, A. H. 2005 Western North Pacific tropical cyclone intensity and ENSO. *Journal of Climate* **18**, 2996–3006. https://doi.org/10.1175/JCLI3457.1.

Chang, C. P., Harr, P. A. & Chen, H. J. 2005 Synoptic disturbances over the equatorial South China Sea and western Maritime Continent during boreal winter. *Monthly Weather Review* **133** (3), 489–503. https://doi.org/10.1175/MWR-2868.1.

Chen, L. S. & Li, Y. 2004 An overview on the study of the tropical cyclone rainfall. In *Proceedings of the International Conference on Storms*, Brisbane. Australian Meteorological and Oceanographic Society, pp. 112–113.

Chen, S. S., Knaff, J. A. & Marks Jr, F. D. 2006 Effects of vertical wind shear and storm motion on tropical cyclone rainfall asymmetries deduced from TRMM. *Monthly Weather Review* **134** (11), 3190–3208. https://doi.org/10.1175/MWR3245.1.

Chen, T. C., Tsay, J. D., Matsumoto, J. & Alpert, J. 2015 Development and formation mechanism of the Southeast Asian winter heavy rainfall events around the South China Sea. Part I: Formation and propagation of cold surge vortex. *Journal of Climate* **28** (4), 1417–1443. https://doi.org/10.1175/JCLI-D-14-00170.1.

Cheung, K., Yu, Z., Elsberry, R. L., Bell, M., Jiang, H., Lee, T. C., Lu, K., Oikawa, Y., Qi, L. & Tsuboki, K. 2018 Recent advances in research and forecasting of tropical cyclone rainfall. *Tropical Cyclone Research and Review* **7** (2), 106–127. https://doi.org/10.6057/2018TCRR02.03.

Compo, G. P., Kiladis, G. N. & Webster, P. J. 1999 The horizontal and vertical structure of east Asian winter monsoon pressure surges. *Quarterly Journal of the Royal Meteorological Society* **125** (553), 29–54. https://doi.org/10.1002/qj.49712555304.

Dare, R. A., Davidson, N. E. & McBride, J. L. 2012 Tropical cyclone contribution to rainfall over Australia. *Monthly Weather Review* **140**, 3606–3619. https://doi.org/10.1175/MWR-D-11-00340.1.

Didlake Jr., A. C. & Houze Jr., R. A. 2013 Dynamics of the stratiform sector of a tropical cyclone rainband. *Journal of the Atmospheric Sciences* **70** (7), 1891–1911. https://doi.org/10.1175/JAS-D-12-0245.1.

Do, Q. V., Do, H. X., Do, N. C. & Ngo, A. L. 2020 Changes in precipitation extremes across Vietnam and its relationships with teleconnection patterns of the Northern Hemisphere. *Water* **12** (6), 1646. https://doi.org/10.3390/w12061646.

Frank, W. M. 1977 The structure and energetics of the tropical cyclone I. Storm structure. *Monthly Weather Review* **105** (9), 1119–1135. https://doi.org/10.1175/1520-0493(1977)105.

Gao, S., Zhai, S., Chen, B. & Li, T. 2017 Water budget and intensity change of tropical cyclones over the western North Pacific. *Monthly Weather Review* **145** (8), 3009–3023. https://doi.org/10.1175/MWR-D-17-0033.1.

Gori, A., Lin, N., Xi, D. & Emanuel, K. 2022 Tropical cyclone climatology change greatly exacerbates US extreme rainfall–surge hazard. *Nature Climate Change* **12** (2), 171–178. https://doi.org/10.1038/s41558-021-01272-7.

Hence, D. A. & Houze Jr, R. A. 2011 Vertical structure of hurricane eyewalls as seen by the TRMM precipitation radar. *Journal of the Atmospheric Sciences* **68** (8), 1637–1652. https://doi.org/10.1175/2011JAS3578.1.

Heo, J.-W., Ho, C.-H., Park, T.-W., Choi, W., Jeong, J.-H. & Kim, J. 2018 Changes in cold surge occurrence over east Asia in the future: Role of thermal structure. *Atmosphere* **9** (6), 222. https://doi.org/10.3390/atmos9060222.

Hersbach, H., Bell, B., Berrisford, P., Hirahara, S., Horányi, A., Muñoz-Sabater, J., Nicolas, J., Peubey, C., Radu, R., Schepers, D., Simmons, A., Soci, C., Abdalla, S., Abellan, X., Balsamo, G., Bechtold, P., Biavati, G., Bidlot, J., Bonavita, M., Chiara, G. D., Dahlgren, P., Dee, D., Diamantakis, M., Dragani, R., Flemming, J., Forbes, R., Fuentes, M., Geer, A., Haimberger, L., Healy, S., Hogan, R. J., Hólm, E., Janisková, M., Keeley, S., Laloyaux, P., Lopez, P., Lupu, C., Radnoti, G., de Rosnay, P., Rozum, I., Vamborg, F., Villaume, S. & Thépaut, J. 2020 The ERA5 global reanalysis. *Quarterly Journal of the Royal Meteorological Society* **146** (730), 1999–2049. https://doi.org/10.1002/qj.3803.

Houze Jr., R. A. 2010 Clouds in tropical cyclones. *Monthly Weather Review* **138** (2), 293–344. https://doi.org/10.1175/2009MWR2989.1.

Huang, H. & Chen, F. 2019 Precipitation microphysics of tropical cyclones over the western North Pacific based on GPM DPR observations: A preliminary analysis. *Journal of Geophysical Research: Atmospheres* **124** (6), 3124–3142. https://doi.org/10.1029/2018JD029454.

Kepert, J. D. 2006 Observed boundary layer wind structure and balance in the hurricane core. Part II: Hurricane Mitch. *Journal of the Atmospheric Sciences* **63** (9), 2194–2211. https://doi.org/10.1175/JAS3746.1.

Khouakhi, A., Villarini, G. & Vecchi, G. A. 2017 Contribution of tropical cyclones to rainfall at the global scale. *Journal of Climate* **30** (1), 359–372. https://doi.org/10.1175/JCLI-D-16-0298.1

Kubota, T., Shige, S., Hashizume, H., Aonashi, K., Takahashi, N., Seto, S., Hirose, M., Takayabu, Y. N., Ushio, T., Nakagawa, K., Iwanami, K., Kachi, M. & Okamoto, K. I. 2007 Global precipitation map using satellite-borne microwave radiometers by the GSMaP project: Production and validation. *IEEE Transactions on Geoscience and Remote Sensing* **45** (7), 2259–2275. https://doi.org/10.1109/TGRS.2007.895337.

Kubota, T., Aonashi, K., Ushio, T., Shige, S., Takayabu, Y. N., Kachi, M., Arai, Y., Tashima, T., Masaki, T., Kawamoto, N., Mega, T., Yamamoto, M. K., Hamada, A., Yamaji, M., Liu, G., Oki, R., 2020 Global satellite mapping of precipitation (GSMaP) products in the GPM era. In: *Satellite Precipitation Measurement: Volume 1* (In: Levizzani, V., Kidd, C., Kirschbaum, D. B., Kummerow, C. D., Nakamura, K. & Turk, F. J., eds). Springer International Publishing, pp. 355–373. https://doi.org/10.1007/978-3-030-24568-9_20.

Kunitsugu, M. 2012 Tropical cyclone information provided by the RSMC Tokyo-Typhoon Center. *Tropical Cyclone Research and Review* **1** (1), 51–59.

Kuo, H. C., Lin, Y. L. & Chen, J. H. 1991 The formation of concentric vorticity structures in typhoons. *Journal of the Atmospheric Sciences* **48** (9), 1242–1257. https://doi.org/10.1175/JAS3286.1.

Lavender, S. L. & McBride, J. L. 2021 Global climatology of rainfall rates and lifetime accumulated rainfall in tropical cyclones: Influence of cyclone basin, cyclone intensity and cyclone size. *International Journal of Climatology* **41**, E1217–E1235. https://doi.org/10.1002/joc.6763.

Lin, Y. L., Chiao, S., Wang, T. A., Kaplan, M. L. & Weglarz, R. P. 2001 Some common ingredients for heavy orographic rainfall. *Weather and Forecasting* **16** (6), 633–660. https://doi.org/10.1175/1520-0434(2001)016.

Lonfat, M., Marks Jr., F. D. & Chen, S. S. 2004 Precipitation distribution in tropical cyclones using the Tropical Rainfall Measuring Mission (TRMM) microwave imager: A global perspective. *Monthly Weather Review* **132** (7), 1645–1660. https://doi.org/10.1175/1520-0493(2004)132.

Lonfat, M., Rogers, R., Marchok, T. & Marks Jr, F. D. 2007 A parametric model for predicting hurricane rainfall. *Monthly Weather Review* **2007** (135), 3086–3097. https://doi.org/10.1175/MWR3433.1.

Marks Jr, F. D. 1985 Evolution of the structure of precipitation in Hurricane Allen (1980). *Monthly Weather Review* **113** (6), 909–930. https://doi.org/10.1175/1520-0493(1985)113.

Martinez, J., Nam, C. C. & Bell, M. M. 2020 On the contributions of incipient vortex circulation and environmental moisture to tropical cyclone expansion. *Journal of Geophysical Research: Atmospheres* **125** (21), e2020JD033324. https://doi.org/10.1029/2020JD033324.

Miller, B. I. 1958 Rainfall rates in Florida hurricanes. *Monthly Weather Review* **86** (7), 258–264. https://doi.org/10.1175/1520-0493(1958)086.

Ministry of Natural Resources and Environment (MONRE) - Vietnam 2016 *Climate Change and Sea Level Rise Scenarios for Vietnam*. Vietnam Natural Resources, Environment and Mapping Publishing House, Hanoi, 2016, pp. 1–188 (in Vietnamese)

Ministry of Natural Resources and Environment (MONRE) – Viet Nam 2021 *Climate Change, Sea Level Rise Scenarios for Viet Nam* (in Vietnamese). Viet Nam Natural Resources, Environment and Mapping Publishing, Hanoi, p. 286.

Miyato, N., Iguchi, T. & Oki, R. 2021 Validation of the dual-frequency precipitation radar onboard the global precipitation measurement core observatory. *Journal of Atmospheric and Oceanic Technology* **38** (8), 1351–1367. https://doi.org/10.1109/TGRS.2020.3039978.

Nodzu, M. I., Matsumoto, J., Trinh-Tuan, L. & Ngo-Duc, T. 2019 Precipitation estimation performance by Global Satellite Mapping and its dependence on wind over northern Vietnam. *Progress in Earth and Planetary Science* **6**, 58. https://doi.org/10.1186/s40645-019-0296-8.

Perşoiu, A., Ionita, M. & Weiss, H. 2019 Atmospheric blocking induced by the strengthened Siberian High led to drying in West Asia during the 4.2 ka BP event – A hypothesis. *Climate of the Past* **15** (2), 781–793. https://doi.org/10.5194/cp-15-781-2019.

Pham, N. T. T. & Vu, H. H. 2020 Characteristics of tropical cyclone precipitating system along central coastal region of Vietnam by TRMM and GSMAP data. In: *APAC 2019: Proceedings of the 10th International Conference on Asian and Pacific Coasts, 2019*, Hanoi, Vietnam. Springer, Singapore, pp. 87–91. https://doi.org/10.1007/978-981-15-0291-0_13

Pham-Thanh, H., Ngo-Duc, T., Matsumoto, J., Phan-Van, T. & Vo-Van, H. 2020 Rainfall trends in Vietnam and their associations with tropical cyclones during 1979–2019. *SOLA* **16**, 169–174. doi:10.2151/sola.2020-029.

Qin, N., Wu, L. & Liu, Q. 2021 Evolution of the moat associated with the secondary eyewall formation in a simulated tropical cyclone. *Journal of the Atmospheric Sciences* **78** (12), 4021–4035. https://doi.org/10.1175/JAS-D-20-0375.1.

Ray, K., Balachandran, S. & Dash, S. K. 2022 Challenges of forecasting rainfall associated with tropical cyclones in India. *Meteorology and Atmospheric Physics* **134**, 1–12. https://doi.org/10.1007/s00703-021-00842-w.

Ren, F., Wu, G., Dong, W., Wang, X., Wang, Y., Ai, W. & Li, W. 2006 Changes in tropical cyclone precipitation over China. *Geophysical Research Letters*. https://doi.org/10.1029/2006GL027951.

Richardson, J. C., Torn, R. D. & Tang, B. H. 2022 An analog comparison between rapidly and slowly intensifying tropical cyclones. *Monthly Weather Review* **150** (8), 2139–2156. https://doi.org/10.1175/MWR-D-21-0260.1.

Rodgers, E. B., Chang, S. W. & Pierce, H. F. 1994 A satellite observational and numerical study of precipitation characteristics in western North Atlantic tropical cyclones. *Journal of Applied Meteorology* **33** (2), 129–139. https://doi.org/10.1175/1520-0450(1994)033.

Shapiro, L. J. 1983 The asymmetric boundary layer flow under a translating hurricane. *Journal of the Atmospheric Sciences* **40** (8), 1984–1998. https://doi.org/10.1175/1520-0469(1983)040.

Takagi, H., Anh, L. T., Islam, R. & Hossain, T. T. 2023 Progress of disaster mitigation against tropical cyclones and storm surges: A comparative study of Bangladesh, Vietnam, and Japan. *Coastal Engineering Journal* **65** (1), 39–53. https://doi.org/10.1080/21664250.2022.2100179.

Tan, I., Reeder, M. J., Singh, M. S., Birch, C. E. & Peatman, S. C. 2023 Wet and dry cold surges over the maritime continent. *Journal of Geophysical Research: Atmospheres* **128** (12), e2022JD038196. https://doi.org/10.1029/2022JD038196.

Tran, T. L., Ritchie, E. A., Perkins-Kirkpatrick, S. E., Bui, H. & Luong, T. M. 2022 Future changes in tropical cyclone exposure and impacts in Southeast Asia from CMIP6 pseudo-global warming simulations. *Earth's Future* **10** (12), e2022EF003118. https://doi.org/10.1029/2022EF003118.

Tran-Anh, Q., Ngo-Duc, T., Espagne, E. & Trinh-Tuan, L. 2022 A high-resolution projected climate dataset for Vietnam: Construction and preliminary application in assessing future change. *Journal of Water and Climate Change* **13** (9), 3379–3399. https://doi.org/10.2166/wcc.2022.144.

Tran-Anh, Q., Ngo-Duc, T., Espagne, E. & Trinh-Tuan, L. 2023 A 10-km CMIP6 downscaled dataset of temperature and precipitation for historical and future Vietnam climate. *Scientific Data* **10** (1), 257. https://doi.org/10.1038/s41597-023-02159-2.

Trinh, T. T., Pattiaratchi, C. & Bui, T. 2020 The contribution of forerunner to storm surges along the Vietnam coast. *Journal of Marine Science and Engineering* **8** (7), 508. https://doi.org/10.3390/jmse8070508.

Trinh, T., Do, N., Trinh, L. & Carr, K. 2023 Flood forecasting by means of dynamical downscaling of global NWPs coupling with a hydrologic model at Nong Son-Thanh My River basins. *Journal of Water and Climate Change* **14** (9), 3257–3279. https://doi.org/10.2166/wcc.2023.262.

Trinh-Tuan, L., Matsumoto, J., Tangang, F. T., Juneng, L., Cruz, F., Narisma, G., Santisirisomboon, J., Phan-Van, T., Gunawan, D., Aldrian, E. & Ngo-Duc, T. 2019a Application of quantile mapping bias correction for mid-future precipitation projections over Vietnam. *SOLA* **15**, 1–6. https://doi.org/10.2151/sola.2019-001.

Trinh-Tuan, L., Matsumoto, J., Ngo-Duc, T., Nodzu, M. I. & Inoue, T. 2019b Evaluation of satellite precipitation products over central Vietnam. *Progress in Earth and Planetary Science* **6**, 54. https://doi.org/10.1186/s40645-019-0297-7.

Ushio, T., Sasashige, K., Kubota, T., Shige, S., Okamoto, K. I., Aonashi, K., Inoue, T., Takahashi, N., Iguchi, T., Kachi, M., Oki, R., Morimoto, T. & Kawasaki, Z. I. 2009 A Kalman filter approach to the global satellite mapping of precipitation (GSMaP) from combined passive microwave and infrared radiometric data. *Journal of the Meteorological Society of Japan, Series II* **87A**, 137–151. https://doi.org/10.2151/jmsj.87A.137.

Walsh, K. J., McBride, J. L., Klotzbach, P. J., Balachandran, S., Camargo, S. J., Holland, G., Knutson, T. R., Kossin, J. P., Lee, T., Sobel, A. & Sugi, M. 2016 Tropical cyclones and climate change. *Wiley Interdisciplinary Reviews: Climate Change* **7** (1), 65–89. https://doi.org/10.1002/wcc.371.

Wang, B. & Zhou, X. 2008 Climate variation and prediction of rapid intensification in tropical cyclones in the western North Pacific. *Meteorology and Atmospheric Physics* **99** (1), 1–16. https://doi.org/10.1007/s00703-006-0238-z.

Wang, S.-Y. S., Promchote, P., Truong, L. H., Buckley, B., Li, R., Gillies, R., Trung, N. T. Q., Guan, B. & Minh, T. T. 2015 Changes in the autumn precipitation and tropical cyclone activity over central Vietnam and its East Sea. *Vietnam Journal of Earth Sciences* **36** (4), 489–496. https://doi.org/10.15625/0866-7187/36/4/6437.

Wang, L., Gu, X. & Beck, H. E. 2021 Cyclones and global floods from an observation–simulation evaluation: Contributions and long-term changes. *Water* **13** (21), 2965. https://doi.org/10.3390/w13212965.

Wexler, H. 1947 Structure of hurricanes as determined by radar. *Annals of the New York Academy of Sciences* **48** (8), 821–845. https://doi.org/10.1111/j.1749-6632.1947.tb38495.x.

Wingo, M. T. & Cecil, D. J. 2010 Effects of vertical wind shear on tropical cyclone precipitation. *Monthly Weather Review* **138** (2), 645–662. https://doi.org/10.1175/2009MWR2921.1.

Wolf, A., Roberts, W. H. G., Ersek, V., Johnson, K. R. & Griffiths, M. L. 2020 Rainwater isotopes in central Vietnam controlled by two oceanic moisture sources and rainout effects. *Scientific Reports* **10** (1), 16482. https://doi.org/10.1038/s41598-020-73508-z.

Wu, M. C. & Chan, J. C. 1995 Surface features of winter monsoon surges over South China. *Monthly Weather Review* **123** (3), 662–680. https://doi.org/10.1175/1520-0493(1995)123.

Wu, M. C. & Chan, J. C. 1997 Upper-level features associated with winter monsoon surges over South China. *Monthly Weather Review* **125** (3), 317–340. https://doi.org/10.1175/1520-0493(1997)125.

Ying, Y. & Zhang, Q. 2012 A modeling study on tropical cyclone structural changes in response to ambient moisture variations. *Journal of the Meteorological Society of Japan, Series II* **90** (5), 755–770. https://doi.org/10.2151/jmsj.2012-512.

Yokoi, S. & Matsumoto, J. 2008 Collaborative effects of cold surge and tropical depression-type disturbance on heavy rainfall in central Vietnam. *Monthly Weather Review* **136** (9), 3275–3287. https://doi.org/10.1175/2008MWR2456.1.

Yu, Z., Wang, Y. & Xu, H. 2015 Observed rainfall asymmetry in tropical cyclones making landfall over China. *Journal of Applied Meteorology and Climatology* **54** (1), 117–136. https://doi.org/10.1175/JAMC-D-13-0359.1.

Zhang, Y., Sperber, K. R. & Boyle, J. S. 1997 Climatology and interannual variation of the East Asian winter monsoon: Results from the 1979–95 NCEP/NCAR reanalysis. *Monthly Weather Review* **125** (10), 2605–2619. https://doi.org/10.1175/1520-0493(1997)125.

Zhang, J. A., Rogers, R. F., Reasor, P. D., Uhlhor, E.W. & Marks Jr, F. D. 2013 Asymmetric hurricane boundary layer structure from dropsonde composites in relation to the environmental vertical wind shear. *Monthly Weather Review* **141** (11), 3968–3984. https://doi.org/10.1175/MWR-D-12-00335.1.

First received 4 March 2024; accepted in revised form 8 July 2024. Available online 19 July 2024